LIDAR SYSTEM CALIBRATION USING POINT CLOUD COORDINATES IN OVERLAPPING STRIPS

Ki-In Bang[a]
Ana Paula Kersting[a]
Ayman Habib[a]
Dong-Cheon Lee[b]
[a]Dept. of Geomatics Engineering, University of Calgary, 2500 University Dr. NW, Calgary, Alberta, T2N 1N4, Canada.
[b]Department of Geo-Informatics, Sejong University, Seoul, South Korea
kibang@ucalgary.ca
ana.kersting@ucalgary.ca
ahabib@ucalgary.ca
dclee@sejong.ac.kr

ABSTRACT

LiDAR systems have become a popular technology, which provides fast and accurate acquisition of object space surface models. The process for correcting the LiDAR data, which is distorted by systematic errors, is accomplished either through strip adjustment or LiDAR system calibration. The strip adjustment reduces or eliminates the discrepancies between overlapping strips using the point cloud coordinates. On the other hand, the calibration procedure recovers systematic errors using the LiDAR equation and system raw measurements from the GPS/INS and laser scanner. The advantage of the strip adjustment is that end-users can reduce the discrepancies between overlapping strips, which are caused by systematic errors, without requiring the availability of the system raw measurements. This approach, however, is limited to the overlapping strips that are considered. This paper proposes an alternative calibration method, where the LiDAR point cloud from overlapping strips are utilized and a simplified LiDAR system equation is derived using few reasonable assumptions. A 3D transformation function is applied to the overlapping strips, and the transformation parameters are estimated using the discrepancies between overlapping strips. After this, the estimated parameters are used to determine the correction terms for the initial calibration parameters based on the relationship between the transformation parameters and systematic errors, where the relationship is derived from the simplified LiDAR equation. The correspondence between overlapping strips is also discussed. In this research, areal and linear features are used as alternative primitives. The feasibility of the proposed method and alternative primitives will be investigated through experimental results from real LiDAR data.

INTRODUCTION

A LiDAR system is basically composed of a laser ranging and scanning unit and a position and orientation system (POS), which consists of an integrated differential global positioning system (DGPS) and an inertial measurement unit (IMU). The principle of laser ranging is to measure distances from the sensor to the ground. The GPS system provides position information and the IMU provides attitude information. The coordinates of the LiDAR points are the result of combining the derived measurements from each of its system components, as well as the mounting parameters relating such components. The relationship between the system measurements and parameters is embodied in the LiDAR equation (Vaughn et al., 1996; Schenk, 2001; El-Sheimy et al., 2005), equation 1. As it can be seen in Figure 1, the position of the laser point, $\vec{X}_G$, can be derived through the summation of three vectors ($\vec{X}_o$, $\vec{P}_G$ and $\vec{\rho}$) after applying the appropriate rotations: $R_{yaw,\ pitch,\ roll}$, $R_{\Delta\omega,\Delta\phi,\Delta\kappa}$ and $R_{\alpha,\ \beta}$. In this equation, $\vec{X}_o$ is the vector from the origin of the ground coordinate system to the origin of the IMU coordinate system, $\vec{P}_G$ is the offset between the laser unit and IMU coordinate systems (lever-arm offsets), and $\vec{\rho}$ is the laser range vector whose magnitude is equivalent to the distance from the laser firing point to its footprint. The term $R_{yaw,\ pitch,\ roll}$ stands for the rotation matrix relating the ground and IMU coordinate systems, $R_{\Delta\omega,\Delta\phi,\Delta\kappa}$ represents

the rotation matrix relating the IMU and laser unit coordinate systems (bore-sighting angles), and $R_{\alpha,\beta}$ refers to the rotation matrix relating the laser unit and laser beam coordinate systems with α and β being the mirror scan angles. For a linear scanner, which is the focus of this paper, the mirror is rotated in one direction only leading to zero α angle. The involved quantities in the LiDAR equation are all measured during the acquisition process except for the bore-sighting angles and lever-arm offsets (mounting parameters), which are usually determined through a calibration procedure.

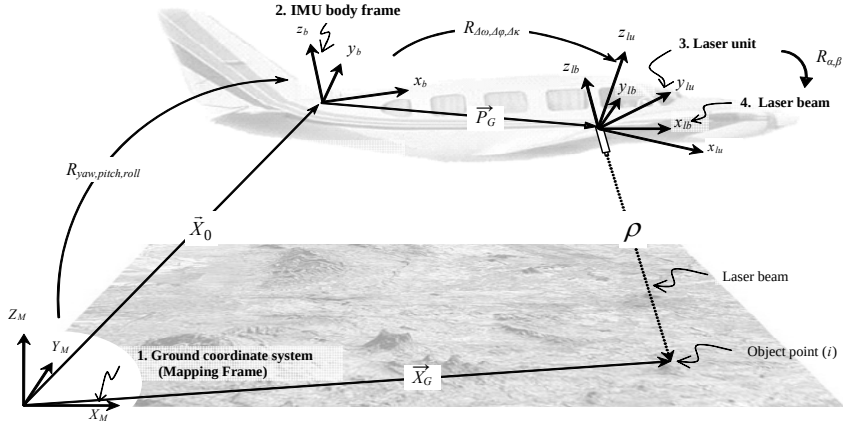

Figure 1. Coordinate systems and involved quantities in the LiDAR equation.

$$\vec{X}_G = \vec{X}_o + R_{yaw,\,pitch,\,roll}\ \vec{P}_G + R_{yaw,\,pitch,\,roll}\ R_{\Delta\omega,\,\Delta\phi,\,\Delta\kappa}\ R_{\alpha,\,\beta}\begin{bmatrix} 0 \\ 0 \\ -\rho \end{bmatrix} \tag{1}$$

The calibration process is usually accomplished in several steps: (i) Laboratory calibration, (ii) Platform calibration, and (iii) In-flight calibration. In the laboratory calibration, which is conducted by the system manufacturer, the individual system components are calibrated. In addition, the eccentricity and misalignment between the laser mirror and the IMU as well as the eccentricity between the IMU and the sensor reference point are determined. In the platform calibration, the eccentricity between the sensor reference point and the GPS antenna is determined. The in-flight calibration utilizes a calibration test field composed of control surfaces for the estimation of the LiDAR system parameters. The observed discrepancies between the LiDAR-derived and control surfaces are used to refine the mounting parameters and biases in the system measurements (mirror angles and ranges). Current in-flight calibration methods have the following drawbacks: (i) They are time consuming and expensive; (ii) They are generally based on complicated and sequential calibration procedures; (iii) They require some effort for surveying the control surfaces; (iv) Some of the calibration methods involve manual and empirical procedures; (v) Some of the calibration methods require the availability of the LiDAR raw measurements such as ranges, mirror angles, as well as position and orientation information for each pulse (Filin, 2001; and Skaloud and Lichti, 2006); and (vi) There is no commonly accepted methodology since the calibration techniques are usually based on a manufacturer-provided software package and the expertise of the LiDAR data provider. As a result of the non-transparent and sometimes empirical calibration procedures, collected LiDAR data might exhibit systematic discrepancies between conjugate surface elements in overlapping strips.

The elimination and/or reduction of the effect of systematic errors in the system parameters and measurements have been the focus of LiDAR research in the past few years. The existing approaches can be classified into two main categories: system driven (calibration) and data driven (strip adjustment) methods. System driven (or calibration) methods (Filin, 2001; Morin, 2002; Skaloud and Lichti, 2006; Friess, 2006), which are considered by many researchers as the ideal solution, are based on the physical sensor model relating the system measurements/parameters to the ground coordinates of the LiDAR points. These methods require the original observations (GPS, IMU, and the laser measurements) or at least the trajectory and time-tagged point cloud (Burman, 2000; Toth, 2002), which might not be directly available to the end-user. Due to that fact, several approaches relying solely on the LiDAR point cloud coordinates, categorized as data-driven methods (or strip

adjustment methods), have been proposed by several authors (Kilian et al., 1996; Crombaghs et al., 2000; Maas, 2002; Bretar et al., 2004; Vosselman, 2004; Filin and Vosselman, 2004; Pfeifer et al., 2005; Kager, 2004). In this type of approach, the effects of the errors onto the point cloud are usually modeled by straightforward transformations between the laser strip coordinate system and a reference coordinate system.

The main objective of this paper is to present a new calibration procedure for the determination of biases in the mounting parameters that overcomes the limitation of existing calibration procedures in terms of requirements of raw LiDAR data. The proposed procedure makes use of the LiDAR point cloud from parallel LiDAR strips with moderate flight dynamics (for example acquired by fixed wing platform) over an area with moderately varying elevation. The system biases are estimated using the identified discrepancies between conjugate primitives in overlapping LiDAR strips. Due to the irregular nature of the LiDAR points, appropriate primitives that can be extracted with a satisfactory level of automation (that is, requiring minimum user interaction) are implemented. Moreover, the appropriate mathematical model relating conjugate surface elements in overlapping parallel strips in the presence of systematic errors in the mounting parameters is investigated. To satisfy the set objectives, one should address the following questions:

(1) What is the impact of errors in the mounting parameters on the mathematical relationship between conjugate surface elements in overlapping parallel strips?
(2) What are the appropriate primitives, which can be identified in overlapping strips?
(3) How to extract and match conjugate primitives with a satisfactory level of automation?
(4) How to utilize the matched primitives for estimating the necessary transformation parameters to determine the biases in the system mounting parameters?

To address these questions, the paper starts with an analysis of systematic errors in the mounting parameters and their impact on the resulting surface. Then, the proposed calibration procedure, including the extraction and matching of the appropriate primitives, is presented. Finally, the paper presents some conclusions and recommendations for future work.

LiDAR ERROR BUDGET

The accuracy of the derived point cloud from a LiDAR system depends on systematic and random errors in the system parameters and measurements. Random errors, regardless of their magnitude, will not lead to systematic discrepancies between conjugate surface elements in overlapping strips. Systematic errors, on the other hand, will result in inconsistencies among neighbouring strips. A detailed description of LiDAR errors can be found in Huising and Pereira (1998), Baltsavias (1999), Schenk (2001), Katzenbeisser (2003), and Glennie (2007). In this section, the impact of systematic errors/biases in the mounting parameters on the derived point cloud is investigated. The impact of systematic errors in the mounting parameters will be evaluated through mathematical analysis of the LiDAR equation. More specifically, the LiDAR equation will be differentiated with respect to the bias-contaminated parameter. In the proposed analysis, the following assumptions are made: a) the flight lines are parallel to the *Y*-axis of the ground coordinate system, b) the LiDAR system is almost vertical and has constant attitude (that is, $R_{yaw,\ pitch,\ roll} \approx$ identity matrix for a system flying along the positive direction of the *Y*-axis), c) a linear scanner with the mirror scanning across the flight line is investigated, d) the LiDAR system has relatively small bore-sighting angles, and e) the mapped area is comprised of a relatively flat terrain, where the height variations are much smaller than the flying height above ground (that is, LiDAR strips cover an area with moderately varying elevation). Such assumptions would simplify the LiDAR geometric model as represented by equation (1) to the form in equations (2). One should note that the scan angle (β) and the lateral distance (x) for a given point are defined relative to the flight trajectory. Therefore, one should use the appropriate signs when dealing with two flight lines, which are flown in opposite directions as shown in Figure 2.

$$\vec{X}_G \approx \vec{X}_o + \begin{bmatrix}\Delta X\\ \Delta Y\\ \Delta Z\end{bmatrix} + \begin{bmatrix}1 & -\Delta\kappa & \Delta\phi\\ \Delta\kappa & 1 & -\Delta\omega\\ -\Delta\phi & \Delta\omega & 1\end{bmatrix}\begin{bmatrix}-\rho\sin(S\ \beta)\\ 0\\ -\rho\cos(S\ \beta)\end{bmatrix} = \vec{X}_o + \begin{bmatrix}\Delta X\\ \Delta Y\\ \Delta Z\end{bmatrix} + \begin{bmatrix}1 & -\Delta\kappa & \Delta\phi\\ \Delta\kappa & 1 & -\Delta\omega\\ -\Delta\phi & \Delta\omega & 1\end{bmatrix}\begin{bmatrix}x\\ 0\\ -H\end{bmatrix} \quad (2.a)$$

$$\vec{X}_G \approx \vec{X}_o + \begin{bmatrix}-\Delta X\\ -\Delta Y\\ \Delta Z\end{bmatrix} + \begin{bmatrix}-1 & \Delta\kappa & -\Delta\phi\\ -\Delta\kappa & -1 & \Delta\omega\\ -\Delta\phi & \Delta\omega & 1\end{bmatrix}\begin{bmatrix}-\rho\sin(S\ \beta)\\ 0\\ -\rho\cos(S\ \beta)\end{bmatrix} = \vec{X}_o + \begin{bmatrix}-\Delta X\\ -\Delta Y\\ \Delta Z\end{bmatrix} + \begin{bmatrix}-1 & \Delta\kappa & -\Delta\phi\\ -\Delta\kappa & -1 & \Delta\omega\\ -\Delta\phi & \Delta\omega & 1\end{bmatrix}\begin{bmatrix}x\\ 0\\ -H\end{bmatrix} \quad (2.b)$$

where,

- Equation 2.a is valid for a system flying along the positive direction of the *Y*-axis (this flight line will be denoted as the forward strip),
- Equation 2.b is valid for a system flying along the negative direction of the *Y*-axis (this flight line will be denoted as the backward strip),
- $\Delta X, \Delta Y, \Delta Z$ are the components of the lever arm offset vector $\vec{P}_G$,
- *S* is a scale factor for the mirror angle β (this scale factor should be unity for a bias-free system),
- *H* is the flying height above ground, and
- *x* is the lateral distance between the LiDAR footprint in question and the projection of the flight trajectory onto the ground.

(a) (b)

Figure 2. Scan angle (a) and lateral distance (b) definitions for two flight lines, which are flown in opposite directions.

In this work, the impact of biases in the lever-arm offset parameters $(\delta\Delta X, \delta\Delta Y, \delta\Delta Z)$ and bore-sighting angles $(\delta\Delta\omega, \delta\Delta\phi, \delta\Delta\kappa)$ is investigated. Differentiating equation (2) with respect to the lever-arm offset parameters, one can see that biases in these parameters $(\delta\Delta X, \delta\Delta Y, \delta\Delta Z)$ will lead to constant shifts in the derived point cloud, equation (3). The magnitudes of these shifts are equivalent to the introduced biases in the lever-arm offset parameters. The approximate equality in equation (3) is used to indicate that it is only valid under the abovementioned assumptions. The multiple signs (±) indicate the impact for the forward and backward strips (with the positive sign referring to the forward strip and the negative sign referring to the backward strip). Therefore, the shifts in the *XY*-directions are dependent on the flying direction. The shift in the *Z*-direction, on the other hand, is independent of the flying direction. Moreover, the planimetric and vertical shifts are independent of the flying height and scan angle.

$$\begin{bmatrix} \delta X_G \\ \delta Y_G \\ \delta Z_G \end{bmatrix}_{\delta\Delta X, \delta\Delta Y, \delta\Delta Z} \approx \begin{bmatrix} \pm\,\delta\Delta X \\ \pm\,\delta\Delta Y \\ \delta\Delta Z \end{bmatrix} \tag{3}$$

Now, the focus will be shifted towards the impact of biases in the bore-sighting angles $(\delta\Delta\omega, \delta\Delta\phi, \delta\Delta\kappa)$, which will be denoted as the bore-sighting pitch, roll, and heading biases, respectively (considering that the flight line is parallel to the Y-axis). The introduced shifts in the ground coordinates of the derived point cloud due to biases in the bore-sighting angles are shown in equation (4). It should be noted that the multiple signs $(\pm, \mp)$ in this equation signify the impacts for forward and backward strips with the top sign always corresponding to the forward strip. Combining the effects of the various biases would lead to the mathematical expression in equation (5). The terms (X_{Biased}, Y_{Biased}, Z_{Biased}) in this equation refer to the bias-contaminated coordinates of the LiDAR point while (X_T, Y_T, Z_T) refer to the true location of the same point.

$$\begin{bmatrix} \delta X_G \\ \delta Y_G \\ \delta Z_G \end{bmatrix}_{\delta\Delta\omega, \delta\Delta\phi, \delta\Delta\kappa} \approx \begin{bmatrix} \mp\ H\ \delta\Delta\phi \\ \pm H\ \delta\Delta\omega \pm\ x\ \delta\Delta\kappa \\ -\ x\ \delta\Delta\phi \end{bmatrix} \tag{4}$$

$$\begin{bmatrix} \delta X_G \\ \delta Y_G \\ \delta Z_G \end{bmatrix}_{Total} = \begin{bmatrix} X_{Biased} - X_T \\ Y_{Biased} - Y_T \\ Z_{Biased} - Z_T \end{bmatrix} \approx \begin{bmatrix} \pm \delta\Delta X \mp H\ \delta\Delta\phi \\ \pm \delta\Delta Y \pm H\ \delta\Delta\omega \pm x\ \delta\Delta\kappa \\ \delta\Delta Z - x\ \delta\Delta\phi \end{bmatrix} \tag{5}$$

Due to the presence of systematic errors in the mounting parameters, the bias-contaminated coordinates of conjugate points in overlapping strips will show systematic discrepancies. The mathematical relationship between these points can be derived by rewriting equation (5) for two overlapping strips and subtracting the resulting equations from each other. An example of such a relationship for two strips, which are flown in opposite directions, is given in equations (6), (7), and (8). It should be noted that equation (6) refers to the forward strip (denoted by the subscript A) while equation (7) refers to the backward strip (denoted by the subscript B). The term D in equation (8) refers to the lateral distance between the two flight lines in question.

$$\begin{bmatrix} X_A - X_T \\ Y_A - Y_T \\ Z_A - Z_T \end{bmatrix} \approx \begin{bmatrix} \delta\Delta X - H\delta\Delta\phi \\ \delta\Delta Y + H\delta\Delta\omega + x_A\,\delta\Delta\kappa \\ \delta\Delta Z - x_A\delta\Delta\phi \end{bmatrix} \tag{6}$$

$$\begin{bmatrix} X_B - X_T \\ Y_B - Y_T \\ Z_B - Z_T \end{bmatrix} \approx \begin{bmatrix} -\delta\Delta X + H\delta\Delta\phi \\ -\delta\Delta Y - H\delta\Delta\omega - x_B\,\delta\Delta\kappa \\ \delta\Delta Z - x_B\delta\Delta\phi \end{bmatrix} \tag{7}$$

$$\begin{bmatrix} X_A - X_B \\ Y_A - Y_B \\ Z_A - Z_B \end{bmatrix} \approx \begin{bmatrix} 2\delta\Delta X - 2H\delta\Delta\phi \\ 2\delta\Delta Y + 2H\delta\Delta\omega + (x_A + x_B)\,\delta\Delta\kappa \\ -(x_A - x_B)\delta\Delta\phi \end{bmatrix} == \begin{bmatrix} 2\delta\Delta X - 2H\delta\Delta\phi \\ 2\delta\Delta Y + 2H\delta\Delta\omega - D\,\delta\Delta\kappa \\ -(x_A - x_B)\delta\Delta\phi \end{bmatrix} \tag{8}$$

Equation (8) can be rewritten after mathematical manipulation to produce the form in equation (9), where the coordinates of a given point in the forward strip is expressed in terms of the coordinates of the corresponding point in the backward strip. The coordinates of the involved points are referred to a local coordinate system whose Y-axis is half-way between the two strips. This local coordinate system can be derived by shifting the origin to the centroid of the point cloud in the overlap area between the strips in question. It should be noted that the rotation matrix in equation (9) corresponds to a rotation around the flight direction (that is, roll angle).

$$\begin{bmatrix} X_A \\ Y_A \\ Z_A \end{bmatrix} = \begin{bmatrix} 2\ \delta\Delta X - 2\ H\ \delta\Delta\phi \\ 2\,\delta\Delta Y + 2\ H\ \delta\Delta\omega - D\ \delta\Delta\kappa \\ 0 \end{bmatrix} + \mathbf{R}_{2\delta\Delta\phi} \begin{bmatrix} X_B \\ Y_B \\ Z_B \end{bmatrix} \tag{9}$$

In a similar fashion, one can derive equation (10), which expresses the mathematical relationship between the bias-contaminated coordinates of the same object point in two overlapping strips that are flown in the same direction.

$$\begin{bmatrix} X_A \\ Y_A \\ Z_A \end{bmatrix} = \begin{bmatrix} 0 \\ -D\ \delta\Delta\kappa \\ D\ \delta\Delta\phi \end{bmatrix} + \begin{bmatrix} X_B \\ Y_B \\ Z_B \end{bmatrix} \tag{10}$$

Equations 9 – 10 reveal the possibility of identifying the presence of systematic errors in the system parameters and/or measurements by evaluating the discrepancies between conjugate points in overlapping strips, which are flown in the same or opposite directions. Moreover, using these equations, it is possible to determine the flight configuration that maximizes the impact of systematic errors. For example, as it can be seen in equation 10, parallel strips with the least amount of necessary overlap for identifying conjugate surface elements are useful for magnifying the bore-sighting heading and roll biases (this is caused by the large lateral distance D). In addition, higher flying heights are optimal for magnifying the bore-sighting pitch and roll biases. Also, closer inspection of these equations would allow for the determination of an optimal flight configuration design which decouples

various systematic errors. For example, working with four strips which are captured from two flying heights in opposite directions with 100% overlap are optimal for the recovery of the planimetric lever-arm offsets as well as the bore-sighting pitch and roll biases. In addition, two flight lines, which are flown in the same direction with the least overlap possible, are optimal for the recovery of the bore-sighting heading and roll biases. Only a vertical bias in the lever-arm offsets cannot be detected by observing discrepancies between conjugate surface elements in overlapping strips. Such inability is caused by the fact that a vertical bias in the lever-arm offsets produces the same effect regardless of the flying direction, flying height, or scan angle.

In summary, this section presented the impact of biases in the mounting parameters. From such analysis the mathematical relationship between conjugate bias-contaminated points in two flight lines, which are flown in the same or opposite directions was derived (equations 9 and 10). It was established that a four-parameter rigid-body transformation (three shifts and one rotation angle around the flight direction) can be used as the transformation function relating overlapping parallel strips, which are flown in the same or opposite directions, in the presence of biases in the mounting parameters. It should be noted that the derived equations are only valid for the listed assumptions throughout this section.

PROPOSED CALIBRATION PROCEDURE

In this section, the proposed calibration procedure for the determination of the biases in the mounting parameters is described. The introduced approach utilizes parallel LiDAR strips acquired by fixed wing platform over an area with moderately varying elevation. The proposed method requires only the LiDAR point cloud and the system biases are estimated using the detected discrepancies between overlapping LiDAR strips. To reliably evaluate the system biases, one must address the following questions:

- What is the appropriate transformation function relating overlapping strips in the presence of systematic biases in the mounting parameters?
- What is the mathematical model relating the estimated transformation parameters (discrepancies) between LiDAR strips and the system biases?
- What are the appropriate primitives, which can be used to identify conjugate surface elements in overlapping strips comprised of irregular sets of non-conjugate points?
- What is the appropriate similarity measure, which utilizes the involved primitives and the defined transformation function to describe the correspondence of conjugate primitives in overlapping strips?

The answers to the first two questions have been already established in the previous section, where it has been mathematically proven that conjugate points in overlapping strips are related to each other through a transformation function involving constant shifts and a rotation angle across the flight direction. Therefore, a four-parameter rigid-body transformation can be used as the transformation function relating overlapping strips in the presence of the discussed biases. The deviation from zero shifts and rotation indicates the presence of biases in the system parameters. The relationship between the transformation parameters estimated using a rigid body transformation and the system biases is also shown in equations 9 and 10 for strips flown in opposite directions and in the same direction, respectively. The answers to the remaining questions depend on the nature of the utilized primitives. Since there is no point-to-point correspondence in overlapping LiDAR strips, one has to rely on other primitives. The following subsection presents the answers to the above questions as they pertain to the selected primitives.

Primitives Extraction and Matching

Due to the irregular nature of the LiDAR points, no point-to-point correspondence exists between overlapping strips. Therefore, other primitives should be employed. Utilizing areal and linear features is more appropriate since one can assume the correspondence of these primitives in spite of the absence of point-to-point correspondence. For LiDAR data over urban areas, areal and linear features can be automatically identified using segmentation and intersection procedures.

In this work, the areal and linear extraction process starts by selecting on the LiDAR intensity images an area that is believed to include areal and linear features. The user clicks on the centre of the area after defining the radius of a circle, within which the original LiDAR points will be extracted. It should be noted that the LiDAR intensity images are only used for visualization purposes (i.e., the extraction process is based on the original LiDAR data). The user needs to establish the area of interest in one of the strips and the corresponding area in the overlapping

strip is automatically defined. Then, a segmentation technique is used to identify planar patches in the point cloud within the selected area (Kim et al., 2007). This segmentation procedure is performed independently on the point cloud for the overlapping strips. The outcome from such segmentation is aggregated sets of points representing planar patches in the selected area. For the extraction of linear features, neighbouring planar patches are identified and intersected to produce straight-line segments.

The outcome of the extraction procedure is a set of areal and linear features in overlapping strips. Due to the nature of the LiDAR data acquisition (e.g., scan angle, surface normal, surface reflectivity, and occlusions), there is no guarantee that there is one-to-one correspondence between the extracted primitives from overlapping strips. To solve the correspondence problem, one has to utilize the attributes of the extracted primitives. In this work, conjugate planar patches in overlapping strips are matched by checking the distance between the respective centroids and the parallelism of their surface normal. On the other hand, conjugate linear features are automatically matched using the normal distance, parallelism, and the percentage of overlap between candidate lines in overlapping strips. Finally, a graphic visualization of matched planar and linear features is presented to the user for confirmation of the validity of the matched primitives. Having extracted conjugate areal and linear features from overlapping strips, the focus will be shifted towards using these primitives for the estimation of the parameters of the transformation function relating these strips (this will be denoted as the similarity measure in the next section).

Similarity Measure

The formulation of the similarity measure depends on the representation scheme for the involved primitives. In this work, an areal feature will be represented by its centroid together with the orientation of its surface normal. A linear feature, on the other hand, will be represented by its end points. It should be noted that the points representing corresponding areal and linear features are not necessarily conjugate. In this research, a point-based similarity measure, which can deal with non-conjugate points, is proposed. More specifically, a rigid body transformation (equation 11) will be used to relate non-conjugate points from the parallel overlapping strips A (X_A, Y_A, Z_A) and B (X_B, Y_B, Z_B). In other words, non-conjugate points along corresponding areal and linear features will be used in the constraint in equation 11 to derive an estimate of the transformation parameters (X_T, Y_T, Z_T, ϕ). Instead of minimizing the distance between the points, the proposed procedure will minimize the normal distance between conjugate features. In order to compensate for the fact that the points representing corresponding features in overlapping strips are not conjugate, one can manipulate the weight matrices for such points. For the centroid of a planar feature, zero weights will be assigned to that point along the plane. This weight restriction will ensure the minimization of the normal distance between conjugate planar patches in overlapping strips, after applying the estimated transformation parameters. In a similar fashion, zero weight will be assigned to the points defining the linear feature along the line direction. To illustrate the weight restriction procedure, one can consider the case for a point representing the centroid of an areal feature. First, a local coordinate system (UVW) with the U and V axes aligned along the plane is defined. The relationship between the strip coordinate system (XYZ) and the local coordinate system (UVW) can be represented by equation 12. The rotation matrix in that equation is defined using the orientation of the normal to the planar patch including the point in question. The original weight matrix P_{XYZ}, as shown in equation 13, is defined as the inverse of the variance-covariance matrix Σ_{XYZ}, which depends on the accuracy specification of the data acquisition system and the feature extraction procedure. Using the law of error propagation, the weight of that point in the local coordinate system P_{UVW} can be derived according to equation 14. As it has been noted earlier, the weight along the plane normal is the only useful information when working with non-conjugate points along corresponding planar patches. Therefore, the weight matrix can be modified according to equation 15. Finally, the modified weight matrix P'_{XYZ} in the strip coordinate system can be derived according to equation 16. When dealing with linear features, the local coordinate system (UVW) is defined in such a way that the U-axis is aligned along the line in question. Equations 12 – 16 can then be used while replacing equation 15 with equation 17, where the weight is only restricted along the line direction.

$$\begin{bmatrix} X_A \\ Y_A \\ Z_A \end{bmatrix} = \begin{bmatrix} X_T \\ Y_T \\ Z_T \end{bmatrix} + R_\phi \begin{bmatrix} X_B \\ Y_B \\ Z_B \end{bmatrix} \tag{11}$$

$$\begin{bmatrix} U \\ V \\ W \end{bmatrix} = R \begin{bmatrix} X \\ Y \\ Z \end{bmatrix} \tag{12}$$

$$P_{XYZ} = \sum\nolimits_{XYZ}^{-1} \tag{13}$$

$$P_{UVW} = R\, P_{XYZ} R^T = \begin{bmatrix} P_U & P_{UV} & P_{UW} \\ P_{VU} & P_V & P_{VW} \\ P_{WU} & P_{WV} & P_W \end{bmatrix} \tag{14}$$

$$\text{For areal features} \rightarrow P'_{UVW} = \begin{bmatrix} 0 & 0 & 0 \\ 0 & 0 & 0 \\ 0 & 0 & P_W \end{bmatrix} \tag{15}$$

$$P'_{XYZ} = R^T P'_{UVW} R \tag{16}$$

$$\text{For linear features} \rightarrow P'_{UVW} = \begin{bmatrix} 0 & 0 & 0 \\ 0 & P_V & P_{VW} \\ 0 & P_{WV} & P_W \end{bmatrix} \tag{17}$$

The proposed weight restriction in equations 15 and 17 will ensure the minimization of the normal distance between conjugate areal/linear features, after applying the estimated transformation parameters. To illustrate such a minimization, one can consider the case of an areal feature. In the Least Squares Adjustment (LSA) procedure, the unknown parameters are estimated to minimize the weighted sum of squared residuals, as represented by equation 18. The coordinates ($X'_{S_2}, Y'_{S_2}, Z'_{S_2}$) in equation 18 refer to the transformed coordinates of the second strip after applying the estimated shifts and rotations from the LSA procedure. Equations 19 – 20 show that the LSA target function minimizes the weighted sum of the squared normal distances between conjugate planar patches after the manipulation of the weight matrix according to equation 15.

$$\Sigma e^T P e = \min \qquad \textit{Where} \qquad e = \begin{bmatrix} X_{S_1} - X'_{S_2} \\ Y_{S_1} - Y'_{S_2} \\ Z_{S_1} - Z'_{S_2} \end{bmatrix} = \begin{bmatrix} dX \\ dY \\ dZ \end{bmatrix} \tag{18}$$

$$\Sigma \begin{bmatrix} dX & dY & dZ \end{bmatrix} P'_{XYZ} \begin{bmatrix} dX \\ dY \\ dZ \end{bmatrix} \rightarrow \Sigma \begin{bmatrix} dX & dY & dZ \end{bmatrix} R^T P'_{UVW} R \begin{bmatrix} dX \\ dY \\ dZ \end{bmatrix} = \min \tag{19}$$

$$\Sigma \begin{bmatrix} dU & dV & dW \end{bmatrix} P'_{UVW} \begin{bmatrix} dU \\ dV \\ dW \end{bmatrix} \rightarrow \Sigma \begin{bmatrix} dU & dV & dW \end{bmatrix} \begin{bmatrix} 0 & 0 & 0 \\ 0 & 0 & 0 \\ 0 & 0 & P_W \end{bmatrix} \begin{bmatrix} dU \\ dV \\ dW \end{bmatrix} = \sum P_W d_W^2 = \min \tag{20}$$

Where [*dU dV dW*] represent the components of the residual vector [*dX dY dZ*] in the *UVW* coordinate system (i.e., the planar patch local coordinate system with *dW* being along the plane normal). It should be noted that well-distributed planar and linear features with varying orientations are necessary for reliable estimation of the transformation parameters. Once the transformation parameters relating parallel overlapping strips are determined, the biases in the mounting parameters can be estimated using equations 9 and 10 for strips flown in opposite directions and in the same direction, respectively. In these equations, the transformation parameters are expressed as a linear combination of the biases in the LiDAR system. This resulting linear system can then be solved using a least-squares adjustment procedure to derive an estimate of the systematic biases in the data acquisition system.

EXPERIMENTAL RESULTS

The experimental results section aims at testing the validity of the introduced calibration procedure using a real dataset. To perform the experiments, a LiDAR dataset, which was captured by an Optech ALTM 3100 from a flying height of 1000m, was acquired. The data is comprised of three parallel strips with 50% overlap (8803, 8804, and 8805). The average point spacing of the acquired data is approximately 0.75m. The covered site is semi-urban with an area of 5km^2 and contains buildings, trees, roads, bare earth, and grass fields. The height variation range in this area is roughly 100 meters.

The linear and areal features were used to estimate the discrepancies between the strips. Figure 2 shows the location and distribution of the utilized linear and areal features for strips 8803&8804 and strips 8804 & 8805 (Figures 2a and 2b, respectively). It should be noted that the flight lines are parallel to the positive and negative directions of the *X*-axis of the ground coordinate system. The provided formulas in the conducted analysis of the systematic errors and their impact assume that the flight lines are parallel to the *Y*-Axis. Therefore, the estimated parameters using areal and linear features have been recalculated to correspond to a coordinate system where the flight direction is parallel to the *Y*-Axis and are presented in Table 1. We can observe compatible transformation parameters from the linear and areal features methods. Therefore, either of the two procedures can be used to detect discrepancies between overlapping strips. A closer look at the reported numbers in Table 1 reveals a better compatibility between strips 8803 & 8804 than strips 8804 & 8805 (i.e., there is a smaller deviation between the estimated transformation parameters for strips 8804 & 8805 from zero shifts and rotations). The incompatibility between the latter strips is quite obvious in the estimated Y_T shift (almost 80cm). Based on the conducted analysis, the deviation in the Y_T shift for strips 8804 & 8805 is suspected to originate from systematic errors in the bore-sighting pitch and heading angles (these errors would affect the coordinates of the derived point cloud in the flight direction). After consultation with the data provider, it was discovered that the system calibration process assumed that there is no bore-sighting heading error, which led to the bore-sighting pitch angle compensating for the bore-sighting heading angle. The impact of ignoring the bore-sighting heading angle during the calibration process is shown in Figure 3, where the individual and accumulated impacts of the bore-sighting pitch and heading angles are illustrated (Figures 3a and 3b, respectively). Implementing a calibration process, which is based on reducing the incompatibility between strips 8803 and 8804 by adjusting the bore-sighting pitch angle, would lead to the profiles in Figure 3c. As it can be seen in this figure, the incompatibility between strips 8803 and 8804 is reduced, while the incompatibility between strips 8804 and 8805 is magnified (which is obvious in Table 1).

(a) (b)

Figure 2. Extracted linear and areal features for strips 8803 & 8804 (a), for strips 8805 & 8804 (b).

Table 1. Estimated transformation parameters between strips 8803&8804 and strips 8805&8804

	Strips 8803&8804					Strips 8805&8804				
	# of Features	X_T (m)	Y_T (m)	Z_T (m)	Φ (°)	# of Features	X_T (m)	Y_T (m)	Z_T (m)	Φ (°)
Linear Features	11	-0.11	0.02	-0.01	0.0073	10	-0.15	0.88	0.01	0.0029
Areal Features	18	-0.16	0.04	-0.01	0.0091	16	-0.21	0.82	0.00	0.0091

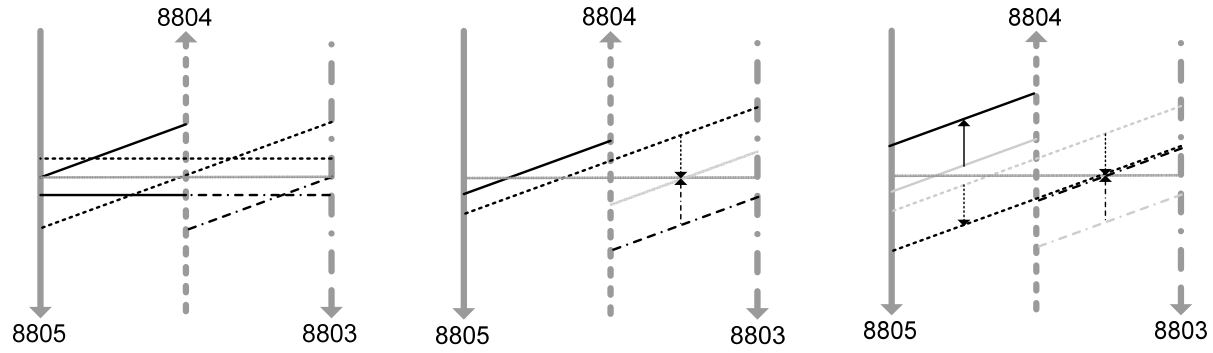

(a) (b) (c)

Figure 3. Individual impact of bore-sighting pitch and heading errors (a), accumulated impact of these errors (b), and resulting surfaces if the incompatibility between strips 8803 & 8804 is removed by adjusting the bore-sighting pitch angle (c).

In order to determine the magnitude of the biases in the mounting parameters, the estimated parameters in Table 1 are then expressed as a linear combination of the biases in the LiDAR system using equation 9 (which corresponds to strips flown in opposite directions). Finally, the resulting equations are used in a least-squares adjustment to derive an estimate of the systematic biases in the data acquisition system and are reported in Table 2 (using the estimated parameters from areal and linear features) where significant biases in the bore-sighting pitch and heading angles are detected, confirming our abovementioned hypothesis. One should note that the estimated biases in Table 2 do not include the bias in the lever-arm offset along the flight direction $(\delta\Delta Y)$. Such a bias could not be decoupled from the bore-sighting pitch bias $(\delta\Delta\omega)$ since the available strips were all captured from the same flying height. Assuming that the lever-arm offsets are much easier to accurately estimate when compared with the bore-sighting angles, $\delta\Delta Y$ is assumed to be zero.

Table 2. Estimated biases in the system parameters using the estimated transformation parameters from the areal and linear features methods

	$\delta\Delta X$ (m)	$\delta\Delta\omega$ (")	$\delta\Delta\phi$ (")	$\delta\Delta\kappa$ (")
Areal Features	-0.02	46	9.2	190
Linear Features	-0.01	44	16	173

CONCLUSIONS AND RECOMMENDATIONS FOR FUTURE WORK

In this work, a new calibration procedure for the estimation of biases in the mounting parameters was introduced. The proposed calibration procedure requires parallel overlapping LiDAR strips acquired by fixed wing platform over an area with moderately varying elevation. The proposed method utilizes only the LiDAR point cloud and the system biases are estimated using the detected discrepancies between overlapping LiDAR strips. The paper started with an analysis of systematic errors in the system mounting parameters and their impact on the derived point cloud coordinates. This analysis has led to the development of a mathematical relationship between conjugate surface elements in overlapping strips. It was demonstrated that a rigid body transformation is an appropriate model for relating conjugate points in parallel overlapping strips acquired by a fixed wing platform in the presence of biases in the mounting parameters. The analysis of systematic errors in LiDAR systems allowed for the derivation of the mathematical model relating the discrepancies between overlapping strips and the biases in the mounting parameters. In addition, it allowed the determination of the optimum flight configuration for decoupling and amplifying the impacts of the systematic errors. Following such an analysis, the paper introduced two methods using linear and areal features for the estimation of the discrepancies between overlapping strips. The performance of the developed model and the calibration procedure has been verified using a real dataset. The results have shown the feasibility of the proposed calibration procedure in operational environments. It was shown that collected LiDAR data might exhibit significant incompatibilities due to insufficient calibration procedures.

Future work will focus on more testing with real data from operational systems. In addition, the impact of biases in the range as well as in the mirror angle measurements will be also investigated. Moreover, the calibration mathematical model will be extended to deal also with non-parallel strips, when navigation data is also available.

ACKNOWLEDGEMENT

This research work has been conducted through funding from the Korean Seoul R&BD program (10541), the Canadian GEOIDE Research Network (SII-43/Phase IV-17), and the Canadian NSERC discovery grant. The authors would also like to acknowledge the University of Calgary Information Technology for providing the real LiDAR data.

REFERENCES

Baltsavias, E., 1999. Airborne laser scanning: existing systems and firms and other resources, *ISPRS Journal of Photogrammetry and Remote Sensing*, 54 (2-3): 164-198.

Bretar F., M. Pierrot-Deseilligny, and M. Roux, 2004. Solving the strip adjustment problem of 3D airborne lidar data, In *Proceedings of the IEEE IGARSS'04,* 20-24 September, Anchorage, Alaska, 7: 4734-4737.

Burman, H., 2000. *Calibration and Orientation of Airborne Image and Laser Scanner Data Using GPS and INS*, Ph.D. dissertation, Royal Institute of Technology, Stockholm,125pages.

Crombaghs, M., E. De Min, and R. Bruegelmann, 2000. On the adjustment of overlapping strips of laser altimeter height data, *International Archives of Photogrammetry and Remote Sensing*, 33(B3/1): 230-237.

El-Sheimy, N., C. Valeo, and A. Habib, 2005. *Digital Terrain Modeling: Acquisition, Manipulation and Applications*, Artech House Remote Sensing Library, 257 pages.

Friess, P., 2006. Toward a rigorous methodology for airborne laser mapping, *Proceedings EuroCOW*. 25-27 January, Castelldefels, Spain. 7 pages (on CD-ROM).

Filin, S., 2001. *Calibration of spaceborne and airborne laser altimeters using natural surfaces*, PhD Dissertation. Department of Civil and Environmental Engineering and Geodetic Science, the Ohio-State University, Columbus, OH, 129 pages.

Filin S., G. Vosselman, 2004. Adjustment of airborne laser altimetry strips, *The International Archives of the Photogrammetry, Remote Sensing and Spatial Information Sciences*, 35 (B3): 285-289.

Glennie, C.L., 2007. Rigorous 3D error analysis of kinematic scanning lidar systems, *Journal of Applied Geodesy*, 1: 147-157.

Huising, E.J. and L.M.G. Pereira, 1998. Errors and accuracy estimates of laser data acquired by various laser scanning systems for topographic applications, *ISPRS Journal of Photogrammetry and Remote Sensing*, 53(5):

245-261.

Kager, H., 2004. Discrepancies between overlapping laser scanning strips- Simultaneous fitting of aerial laser scanner strips, *Proceedings of the International Society for Photogrammetry and Remote Sensing XXth Congress*, Istanbul, 34(B/1): 555 - 560.

Katzenbeisser, R., 2003. About the calibration of lidar sensors, *Proceedings of the ISPRS working group III/3 workshop, 3-D Reconstruction from Airborne Laserscanner and InSAR Data*, Dresden, 6 pages (on CD-ROM).

Kilian, J., N. Haala, and M. Englich, 1996. Capture and evaluation of airborne laser scanner data, *International Archives of Photogrammetry and Remote Sensing*, 31(B3):383–388.

Kim C., A. Habib, P. Mrstik, 2007. New approach for planar patch segmentation using airborne laser data, *Proceedings of the 2007 ASPRS - American Society for Photogrammetry and Remote Sensing, Annual Conference,* Tampa, Florida, 12 pages (on CD-ROM).

Maas H.G., 2002. Method for measuring height and planimetry discrepancies in airborne laserscanner data, *Photogrammetric Engineering and Remote Sensing*, 68(9): 933–940.

Morin, K.W., 2002. *Calibration of Airborne Laser Scanners*, M.S. thesis, University of Calgary, Department of Geomatics Engineering. 125 pages.

Pfeifer, N., S.O. Elberink, and S. Filin, 2005. Automatic tie elements detection for laser scanner strip adjustment, *International Archives of Photogrammetry and Remote Sensing*, 36(3/W3): 1682-1750.

Schenk, T., 2001. Modeling and analyzing systematic errors in airborne laser scanners, *Technical Report in Photogrammetry* No. 19, Ohio Sate University, 42 pages.

Skaloud, J., and D. Lichti, 2006. Rigorous approach to bore-sight self-calibration in airborne laser scanning, *ISPRS Journal of Photogrammetry and Remote Sensing*, 61: 47–59.

Toth, C.K., 2002. Calibrating Airborne Lidar Systems, http://www.isprs.org/commission2/proceedings02/paper/084_100.pdf [Accessed: 15th November 2007].

Vaughn, C.R., J.L. Bufton, W. B. Krabill, and D.L. Rabine, 1996. Georeferencing of aAirborne laser altimeter measurements, *International Journal of Remote Sensing*, 17(11): 2185-2200.

Vosselman, G., 2004. Strip Offset Estimation Using Linear Features, http://www.itc.nl/personal/vosselman/papers/vosselman2002.columbus.pdf [Accessed: 15th November 2007].